Biosensors and Bioelectronics 177 (2021) 112981

Contents lists available at ScienceDirect

Biosensors and Bioelectronics

journal homepage: http://www.elsevier.com/locate/bios

# An enzyme-powered, three-dimensional lame DNA walker

Jie Fang [a,b,1], Changjing Yuan [a,1], Junjie Li [b], Junlong Li [d], Tingyan Yang [b], Yongcan Guo [e], Ding Wang [b], Jianjiang Xue [c,*], WeiLing Fu [a,**], Guoming Xie [b,***]

[a] Department of Laboratory Medicine, Southwest Hospital, Army Medical University (Third Military Medical University), Chongqing, 400038, China
[b] Key Laboratory of Laboratory Medical Diagnostics, Ministry of Education, Department of Laboratory Medicine, Chongqing Medical University, Chongqing, 400016, China
[c] Department of Clinical Laboratory, University-Town Affiliated Hospital of Chongqing Medical University, Chongqing, 401331, China
[d] Department of Endocrinology, The First Affiliated Hospital of Chongqing Medical University, Chongqing, 400016, China
[e] Clinical Laboratory, Traditional Chinese Medicine Hospital Affiliated to Southwest Medical University, Luzhou, 646000, China

ARTICLE INFO

*Keywords:*
Lame DNA walker
Microsphere
Nicking endonuclease
Biosensor

ABSTRACT

Molecular machines constructed by three-dimensional (3-D) DNA walker have emerged as a hot topic in applications such as novel biosensors, cargo delivery platforms and intracellular imaging. Herein, we first propose a lame DNA walker that can randomly and autonomously move on microsphere-based 3-D track. The stochastic lame walker has a long leg mainly responsible for persistent movement and a short leg cutting substrates rapidly. Its motion is propelled by a nicking endonuclease cleavage of hybridized DNA tracks. Kinetic and persistent study show that the lame DNA walker enables reaction equilibrium at 30 min, need a cleat domain of at least 14 nucleotides and can persistently move on 3-D tracks with an average rate of $6.467 \times 10^{-11}$ M $s^{-1}$. We also demonstrate that the lame walker can be used to detect target DNA in the detection range of 10 pM–5 nM with high specificity by toehold exchange mechanism. This work will further expand the performance of 3-D DNA walkers and substantially contributes to the improved understanding of DNA walking systems.

## 1. Introduction

Inspired by both biology and macroscopic engineering, molecular machines using strategies of DNA walkers have been extensively investigated in recent years (Abendroth et al., 2015; Li et al., 2018a; Thubagere et al., 2017; Wang 2009; Yehl et al., 2016; Zhang and Seelig 2011). Typically, these walkers are driven by strand exchange reactions (Gu et al., 2010; Ma et al., 2018; Muscat et al., 2011; Urban et al., 2015), photoactivated reactions (Liu et al., 2014; Loh et al., 2014), DNAzymes (Cha et al., 2014; Pan et al., 2017) and protein enzymes (Feng et al., 2018; Huang et al., 2019; Li et al., 2018b; Tian et al., 2017). The realization of the earliest one-dimensional (1-D) DNA footpaths (Bath et al., 2009; Shin and Pierce 2004; Wang et al., 2015; Yin et al., 2004; You et al., 2012), and two-dimensional (2-D) DNA origami (Fan et al., 2019; Liber et al., 2015; Wang et al., 2017; Wickham et al., 2011; Yang et al., 2015; Zhou et al., 2015), as well as current three-dimensional (3-D) DNA modified particle tracks (Jung et al., 2016; Liang et al., 2017; Xiao et al., 2019; Yang et al., 2016) has released the signal amplification power of DNA walking devices. Among them, 3-D DNA walkers have attracted significant attention with the sustainable advance of nanotechnology and the increased demand for further improvement of DNA walker performance. Applications of these DNA walkers include novel biosensors (Chai and Miao 2019; Li et al., 2018b), intracellular imaging (Liang et al., 2017; Xu et al., 2019) and cargo delivery platforms (Pan et al., 2017; Yang et al., 2016).

In the earlier report, Ellington and co-workers introduced the first 3-D DNA walker based on the principle of catalytic hairpin assembly including the single-catalyst and double catalyst (Jung et al., 2016). Although, the speed of double catalyst walker was faster than that of the single-catalyst, the double catalyst walker had crossed between the microspheres. Besides, as the particle-bound substrate was exhausted, the catalyst readily dissociated from the depleted substrate patch. For the sake of upgrading the persistence, the same group modified the walker design by replacing one catalyst with a cleat domain to prevent it

* Corresponding author.
** Corresponding author.
*** Corresponding author.
*E-mail addresses:* jianjiangxue@126.com (J. Xue), fwl@tmmu.edu.cn (W. Fu), guomingxie@cqmu.edu.cn (G. Xie).
[1] Jie Fang and Changjing Yuan contributed equally to this work.

https://doi.org/10.1016/j.bios.2021.112981
Received 2 November 2020; Received in revised form 28 December 2020; Accepted 4 January 2021
Available online 8 January 2021
0956-5663/© 2021 Elsevier B.V. All rights reserved.

from dissociating from the track, thereby ensuring its higher persistence (Jung et al., 2017). However, the fixed single-legged DNA walker via the cleat sacrificed the walking speed to a large extent, resulting in slow catalytic kinetics that cannot reach equilibrium even after 12 h. In addition to attaching a cleat on the walker, some researchers also fixed walking catalyst on the surface of particles to increase its persistence, thus preventing the catalyst from falling off. For example, Yang et al. designed an enzyme-powered 3-D DNA nanomachine whose walking catalyst was directly attached to gold nanoparticles (Yang et al., 2016). Later, we also successively proposed a two-layer 3-D DNA walker with highly integrated entropy-driven and enzyme-powered reactions based on the similar structure (Yuan et al., 2019). Although these DNA walkers bypass the dissociation, they involve sophisticated track construction that relies largely on the proportion of two different substrates. Therefore, there is still a great demand to develop a 3-D DNA walker with simple design, fast speed and high persistence.

On the basis of previous research foundation and the problems appeared, we herein engineer a new 3-D lame DNA walker. As depicted in Fig. 1, the whole system is composed of only one type of particle-bound substrate, lame catalyst and enzyme, which makes it readily approach the optimal operation condition. Lame DNA walker driven by enzyme consists of a pair of legs with different length but contains the same enzyme recognition site, one is 21 nucleotides (nt) long while the other is only 7 nt, for which we call it lame DNA walker. The long leg is mainly responsible for continuous movement and persistent associate with another track through a unique cleat after enzymatic hydrolysis track, whereas the short leg is designed particularly to stochastic walk on the track and rapidly search for new substrates. Such lame design promotes the persistent fixation of the walking strands on the track and achieves the high kinetics with the concurrent movement of two legs assist. Overall, the simple design meets simultaneously the requirements of high speed and persistence.

## 2. Experimental

### 2.1. Reagents and materials

All oligonucleotides were synthesized and purified with HPLC by Sangon Biotech Inc. (Shanghai, China), and the sequences were shown in Table S1. Streptavidin-coated microsphere suspensions (0.86 μm and 1 μm) were purchased from Spherotech and Bangs Laboratory (Fishers, IN) respectively. Nicking endonuclease Nb.BbvCI and Nt.CviPII, blunt endonuclease AluI and SspI-HF were all purchased from New England Biolabs (Canada). All other chemicals were of analytical grade and were obtained from Sangon Biotech Inc. (Shanghai, China) unless otherwise indicated.

### 2.2. Preparation of Biotin-S-FAM and Biotin-S microspheres

50 μL streptavidin coated microspheres (10 mg microspheres/mL) were washed twice with 50 μL of binding buffer (20 mM Tris, pH 7.5; 1 M NaCl; 1 mM EDTA; 0.0005% Triton X-100) by centrifuging the particles at 12K rpm for 2 min followed by decanting the supernatant. After re-suspending the microspheres in 50 μL of binding buffer, biotin-S-FAM or biotin-S (5 μL, 20 μM) was added into the particles and then incubated for 20 min at 37 °C. After removing any unbound biotinylated

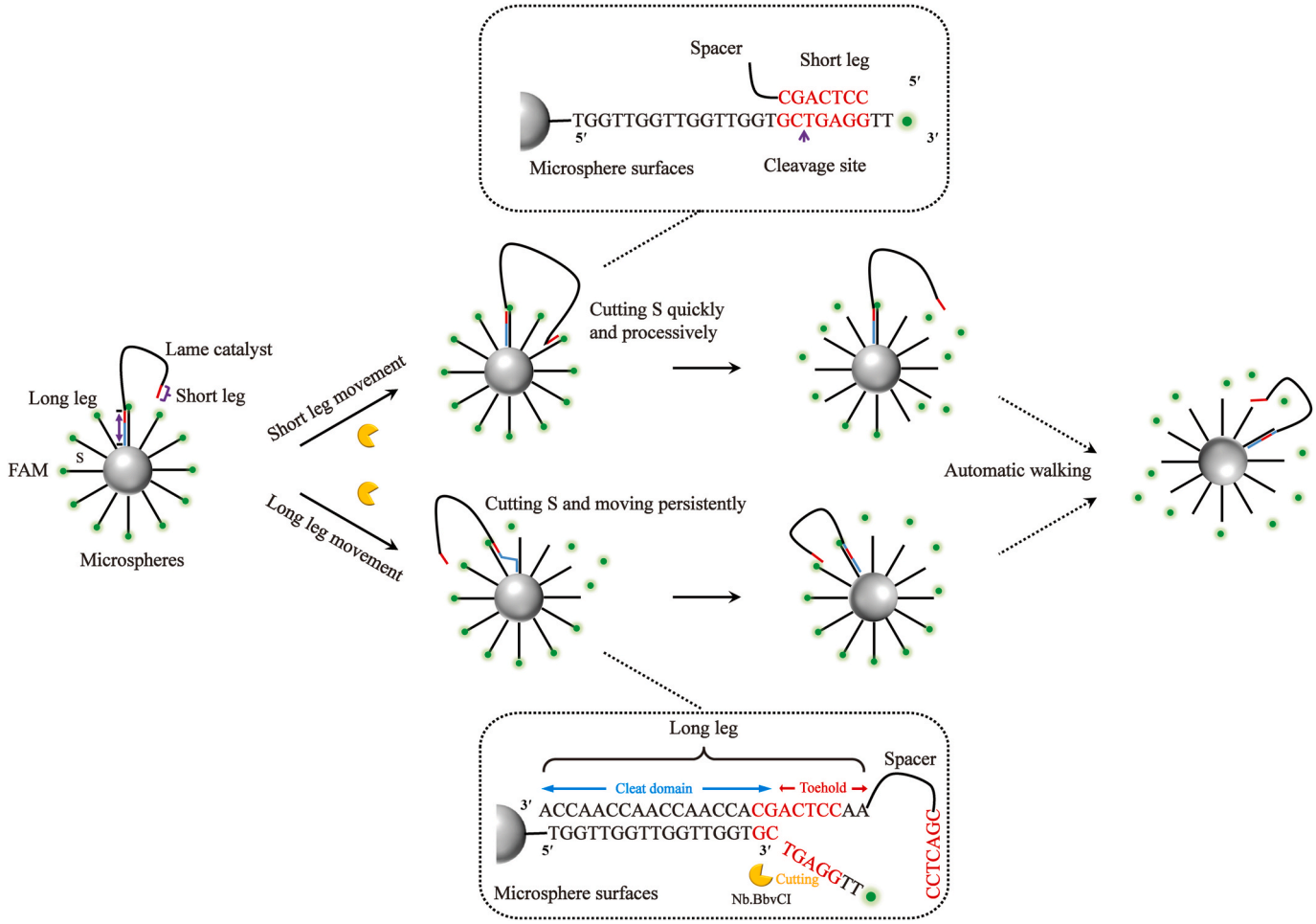


**Fig. 1.** Schematic illustration of a 3-D lame DNA walker that persistently moved along the surface of microspheres.

oligonucleotide by washing twice in 50 μL TE buffer (10 mM Tris-HCl; 1 mM EDTA; pH = 8.0), biotin-S-FAM or biotin-S microspheres were prepared by resuspension with 50 μL of TE buffer.

### 2.3. The walker reaction and fluorescence microscopy imaging on the surface of microspheres

For a typical walker reaction, a reaction mixture containing biotin-S-FAM microspheres (5 μL), various single-legged or lame catalyst (10 μL, final concentration: 5 nM), nicking endonucleases (2 μL, 20 U), 10 × NEB CutSmart buffer (10 μL) and ultrapure water (73 μL) was incubated for appropriate time at 37 °C. After centrifugation, the fluorescence signals in the supernatant were measured by the Cary Eclipse Fluorescence Spectrophotometer (Agilent, California). Fluorescence emission was excited at 480 nm with recording emission range of 500–600 nm.

To monitor the behaviour of the lame catalyst on the microspheres surface, catalyst-primed microspheres and unprimed biotin-S-FAM microspheres were mixed in a ratio of 1:1. The detailed procedure was as follows. The suspension of prepared biotin-S microspheres (5 μL), 10 × NEB CutSmart buffer (10 μL) and ultrapure water (68 μL) were incubated with various lame walkers (10 μL, 5 nM) at 37 °C for 1 h to form catalyst-primed microspheres, followed by the addition of 5 μL of unprimed biotin-S-FAM microspheres. 20 U Nb.BbvCI was then added to a total volume of 100 μL. After incubation at 37 °C for 15 min, the supernatant was taken to detect the fluorescence signals, and the remaining microspheres were resuspended in 50 μL TE buffer for fluorescence microscopy imaging (Nikon 80i, Japan).

### 2.4. DNA detection using the lame DNA walker

Reservoir microspheres were prepared by the same process as for Biotin-S microspheres. Group B *streptococcus* DNA (GBS T) was used as the model target. Bacteria culture, sequencing and GBS T from the whole GBS genome see Supporting Section 1and 2. A certain concentration of GBS T was added to 30 μL NEB CutSmart buffer containing 5 μL reservoir microspheres to react at 37 °C for 60 min. The samples were centrifuged and the supernatants transferred to a new reaction tube including 5 μL synthesized biotin-S-FAM microspheres and 20 U Nb.BbvCI. A lame DNA walker reaction was performed at 37 °C in NEB CutSmart buffer for 60 min. Reactions were stopped by centrifugation at 12K rpm for 2 min, and the fluorescence signals in the supernatant were measured. Reactions without target DNA were taken as the background.

## 3. Results and discussion

### 3.1. Design of the lame DNA walker and operation principle

The design of lame DNA walker is illustrated in Fig. 1. The carboxyfluorescein (FAM)-labeled substrates (S), bearing cleavage sequence of nicking endonuclease (Nb.BbvCI), are interlinked by biotin-streptavidin on the surface of streptavidin-coated microspheres. Specially designed lame catalyst consists of long leg, spacer (A) and short leg. The sequences of both legs are designed to be complimentary to that of the substrates. One is 21 nucleotides (nt) long while the other is only 7 nt. Long leg is further conceptually subdivided into a toehold domain (T) and a cleat domain (C) to elucidate the roles of different domains in the lame catalyst on the microsphere surface. The lame catalyst is driven forward by the hydrolysis of DNA tracks via Nb.BbvCI.

In more detail, based on Watson-Crick base pair basic principle, lame catalyst can interact with S and form complete recognition sites of Nb.BbvCI with high sequence specificity (Huang et al., 2019; Li et al., 2013; Zhang et al., 2019), causing the S to split. For long leg, since the hybridization of seven complementary nucleotides is not stable enough at ambient temperature (Yuan et al., 2019; Zhang et al., 2015), the '5′-TGAGGTT-FAM-3′' signal strand will break away from S and concomitant with the formation of a T domain of long leg. In this state, the C domain keeps lame catalyst in tight contact with S, whereas the newly exposed T domain within long leg can undergo branch migration with adjacent S through toehold exchange, allowing long leg to persistently move on microsphere and release signal strand. During the movement of long leg, as the short leg contains only the enzymatic cleavage sequence, it will randomly and continuously cut S nearby and release signal strand in a much fast speed until all available cleavage sites are used up and reach equilibrium. Overall, the lame walker has two characteristic behaviors: the speedup of the double catalysts reaction and the persistence of the long legs. Finally, the fluorescent signal in supernatant solutions are determined by fluorescence spectrophotometer after centrifugation.

### 3.2. Characterization of the lame DNA walker

Initially, the streptavidin-coated microspheres were analyzed by scanning electron microscope (SEM). Fig. 2B showed a clear magnification image of the microspheres. Obviously, the microspheres were uniform in shape and size with 1 μm average diameter. Then, we performed a feasibility test to determine whether the lame walker could proceed on microsphere surfaces. A catalyst-free control (Fig. 2, Blank) was studied with S modified microspheres and Nb.BbvCI. It was observed that lame walker displayed a stable and low background fluorescence (4.306 a.u.), depending on the specific enzymatic property, powerful streptavidin-biotin bond and the strong elution ability of TE buffer, which minimized the nonspecific adsorption between S and microspheres (Fig. S1). A successful reaction activated by the lame walker should cause a large amount of S far away from the microsphere surfaces, thus enhancing the fluorescence of the supernatant. In lame walker reactions, the 60-min fluorescence intensity of the C domain with length of 8 (LC8, with a 7 base of toehold domain) and 14 (LC14) increased remarkably by a factor of 62.643 (Figs. 2C) and 60.445 (Fig. 2D), respectively, indicating a success of lame walker proceed on microsphere surfaces. Besides, the signal-to-noise ratio calculated by the lame walker was more than 60-fold, with the highest rate recorded in the existing 3-D DNA walkers (Table 1). High signal-to-noise ratio means it can detect targets of the same concentration with greater discrimination.

### 3.3. Kinetic study of the 3-D lame walker

Comparative experiment between lame walker (L) and one-legged walker (O) (scheme in Fig. 2A) was studied to demonstrate the superiority of the lame walker by the ratio of the final fluorescence increased at 60 min. Fig. 2C showed that the fluorescence intensity was 1.134 times high in lame walker (LC8) as that in one-legged walker with the same length of C domain (OC8). But when the length of C domain was 14, the ratio reached to 1.539 in Fig. 2D, suggesting that the length of C domain is of great significance to lame walker. In order to verify the merits of lame walker over one-legged walker more intuitively, a kinetic study was carried out by monitoring the fluorescence increase every 20 min for totally 160 min (Fig. 2E). Remarkably, 5 nM of lame catalyst LC14 (red line) reached equilibrium at 30 min, while the one-legged catalyst OC14 with the same concentration required about 120 min (green line). The average rates of the lame and one-legged walker reaction were measured to be $6.467 \times 10^{-11}$ M $s^{-1}$ and $3.025 \times 10^{-11}$ M $s^{-1}$, respectively. To obtain the average rate, the difference in fluorescence in the absence and presence of the walker was divided by 20 min (Supporting Section 3). These results sufficiently reveal that the lame walker is superior to the one-legged walker. The average rate of lame walker also had advantages in stochastic DNA walker (roughly estimated at $4.43 \times 10^{-12}$ M $s^{-1}$, Supporting Section 3), endogenous stimulus-based walker ($3.7 \times 10^{-12}$ M $s^{-1}$) (Ma et al., 2018) and other enzyme-driven walker ($5.72 \times 10^{-11}$ M $s^{-1}$) (Yang et al., 2016).

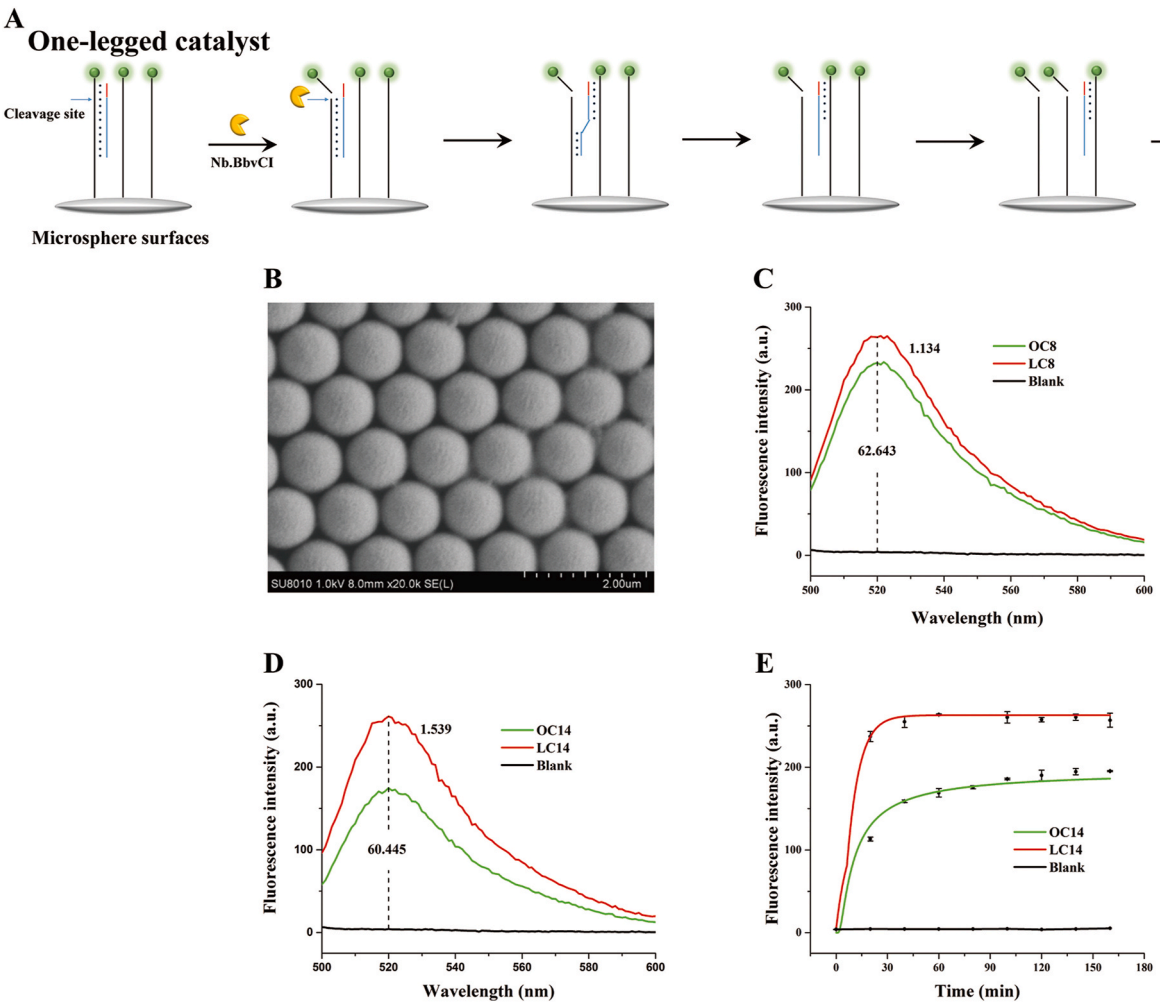


**Fig. 2.** (A) Schematic illustrating the principle of one-legged DNA walker that moved on the microsphere surfaces. (B) SEM image of clustered streptavidin-coated microspheres (SU8010, Japan). The analysis of fluorescence emission spectra of substrates hydrolysis on the microspheres by 8-nt length of the C domain (C) (5 nM LC8, red; 5 nM OC8, green; Blank, without walker) and 14-nt length of the C domian (D) (5 nM LC14, red; 5 nM OC14, green; Blank, without walker). (E) Monitoring the fluorescence increase as a function of time in response to lame DNA walker (5 nM LC14, red), one-legged DNA walker (5 nM OC14, green) and background (without walker, black). Error bars represented one standard deviation from triplicate analyses. (For interpretation of the references to colour in this figure legend, the reader is referred to the Web version of this article.)

**Table 1**
Comparison between lame walker and other 3-D DNA walkers.

| Type | Catalyst | Track substrates | Concentration of catalyst | Reaction time (min) | Signal-to-noise ratio | Linear range | Sensitivity |
|---|---|---|---|---|---|---|---|
| Stochastic DNA walker (Jung et al., 2016) | Two-legged catalyst | A type of DNA | 2 nM | 120 | ~6.7 | / | 0.01–1 nM |
| Two-layer walker (Yuan et al., 2019) | One-legged catalyst | Sophisticated track | 5 nM | 60 | 13.4 | 2 pM-5 nM | 2 pM |
| Enzyme-powered 3-D walker (Yang et al., 2016) | One-legged catalyst | Sophisticated track | 5 nM | 60 | ~8 | 5 pM-5 nM | 5 pM |
| Endogenous stimulus-based walker (Ma et al., 2018) | One-legged catalyst | Sophisticated track | 5 nM | 60 | ~8 | 100 pM-2 nM | 100 pM |
| Entropy-driven walker (Liang et al., 2017) | One-legged catalyst | Sophisticated track | 5 nM | 60 | 16.8 | 20 pM-10 nM | 8 pM |
| Enzyme-free DNA walker (Li et al., 2017) | Two-legged catalyst | A type of DNA | 1 nM | 90 | 15 | 50 pM −1 nM | 6.5 pM |
| Nonenzymatic DNA nanomachine (Zheng et al., 2018) | Two-legged catalyst | A type of DNA | 0.37 nM | 180 | ~5 | 15 pM–370 pM | 3.4 pM |
| Lame walker (this work) | lame catalyst | A type of DNA | 5 nM | 30 | 60.4 | 10 pM-5 nM | 10 pM |

### *3.4. Study on the persistence of the lame DNA walker*

Since the persistence of lame walker was determined by its long leg, the C domain with different lengths of 2 (LT7C2), 4 (LT7C4), 8 (LT7C8), 12 (LT7C12), 14 (LT7C14) and 16 (LT7C16) were designed to evaluate the performance of lame walker reaction. Considering that the

saturation time of LT7C2 and LT7C4 should be shorter than that of LC14 (30 min), fluorescence intensity detection in a shorter time (15 min) was required to identify the performance of different walkers. As shown in Fig. 3B, the shorter the length of C domain (LT7C2, LT7C4 and LT7C8), the higher the fluorescence intensity of lame walker (261.212 a.u., 259.877 a.u. and 242.030 a.u.), which indicated that double catalyst walker with equal-length legs (LT7C2) had an advantage over lame walker in speed. This was because the shorter C domain could initiate branch migration with adjacent tracks more rapidly. But at the same time, they may be more likely to fall off from the original microsphere surface, resulting in their relatively low persistence. The longer the length of C domain, the stronger the bond between S and lame catalyst, and the longer the persistence of the walker. However, the longer C domain was the rate limiting step of the overall branch migration, it was slower in toehold mediated branch migration between the long leg and the new S, thus causing lower fluorescence (LT7C12, 178.532 a.u.; LT7C14, 155.608 a.u.; LT7C16, 136.758 a.u.). Therefore, it was necessary to find an appropriate length of cleats to balance lame walker's speed and persistence.

Given that an effective lame walker should traverse on the pre-designed tracks with minimal dissociation, an additional experiment was conducted. The catalyst-primed microspheres not labeled FAM and unprimed microspheres labeled FAM (biotin-S-FAM microspheres) were uniformly mixed in a ratio of 1:1 (Fig. 3A). Walking in the presence of different lengths of C domain was initiated by adding Nb.BbvCI. The fluorescence of separated supernatant and the remaining washed microspheres and the corresponding results were available by fluorescence spectrophotometer and fluorescence microscope respectively. If lame walker was persistent, lame catalyst should not be transferred from microspheres primed with lame catalyst to adjacent unprimed fluorescent microspheres, which will result in no fluorescence detected in the supernatant, in relative terms, abundant of fluorescent microspheres will be observed under the microscope. As shown in Fig. 3C, short C domain caused masses of fluorescence because of catalyst leakage (LT7C2, 156.766 a.u.; LT7C4, 149.804 a.u.; LT7C8, 138.276 a.u.). For lame catalyst LT7C12, a slight increase in fluorescence signal was observed (38.682 a.u.). When longer C domain was introduced, lame walkers LT7C14 and LT7C16 were hardly released and the fluorescence signal remained nearly unchanged (21.530 a.u. and 19.319 a.u.). The fluorescence microscopic analysis showed that almost no green fluorescence dots were observed in lame catalyst LT7C4 (Fig. 3C) and LT7C8 (Fig. 3D), but remaining microspheres of lame catalyst LT7C14 existed in a distribution of bright green fluorescent dots (Fig. 3F), which matched well with the results of supernatant, that is, the lame catalyst remained attached to the original microsphere. So, for the sake of the balance between speed and persistence, LT7C14 with very little leakage but a higher speed was preliminary selected as the research condition.

Additionally, 20 base pairs (bp) of C domain lengths were required to achieve the best persistent state in previous persistence studies (Jung et al., 2017). However, we observed that the optimum length of C

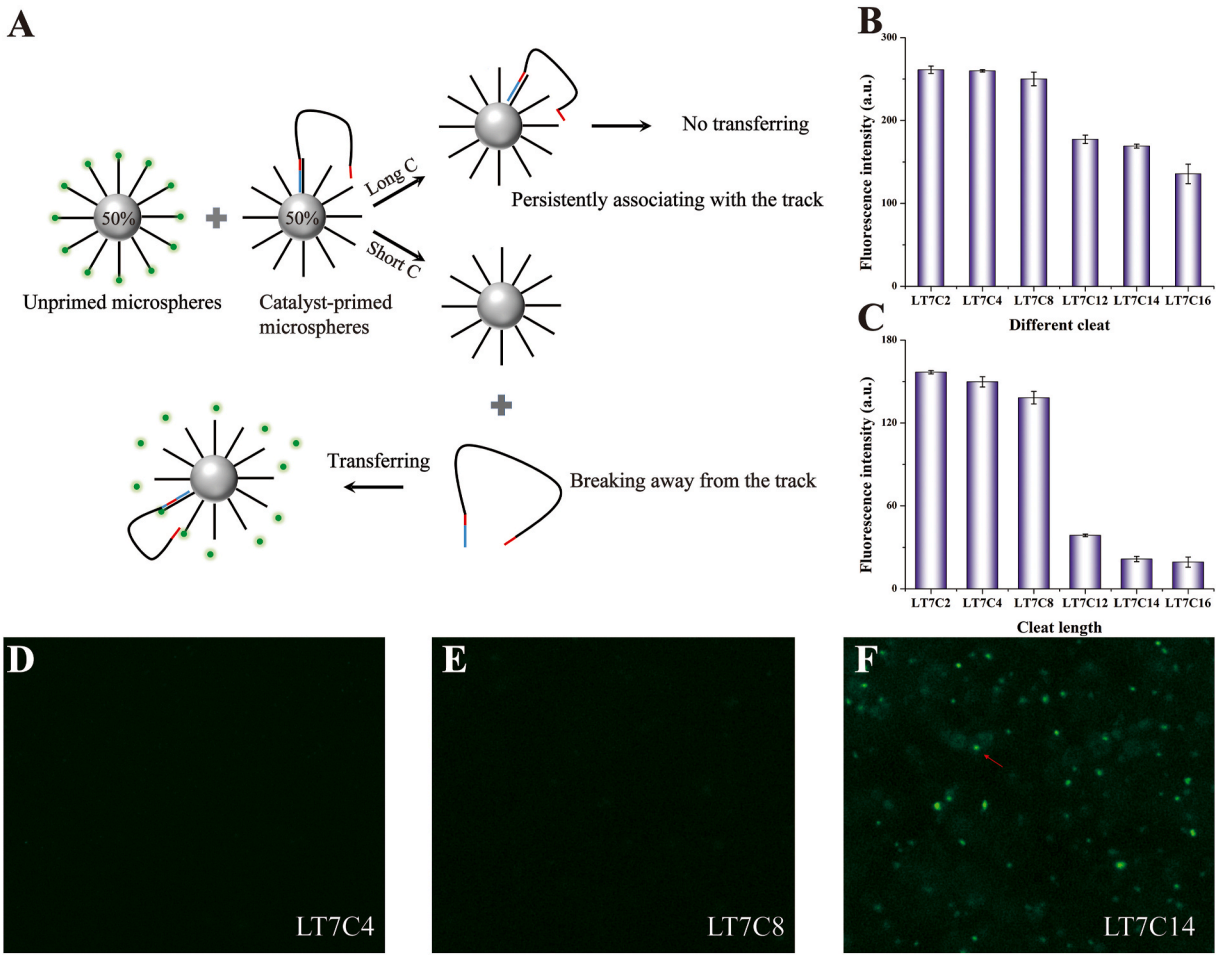


**Fig. 3.** Study on the persistence of the lame DNA walker. (A) Schematic illustration of the design of persistent assay. (B) The performance of the lame walker for designs bearing different lengths of C domain (5 nM LT7C2, LT7C4, LT7C8, LT7C12, LT7C14 and LT7C16). (C) Effect of C domian length on the persistence (5 nM LT7C2, LT7C4, LT7C8, LT7C12, LT7C14 and LT7C16). (D–F) Fluorescence images showing a lawn of FAM-labeled microspheres for various lame catalysts (LT7C4, LT7C8 and LT7C14). The arrow indicated the region where microspheres took on green fluorescence. Error bars represented one standard deviation from triplicate analyses. (For interpretation of the references to colour in this figure legend, the reader is referred to the Web version of this article.)

domain of lame walker for persistence was 14, 6 bases less than expected. We reasoned that with the aid of short leg, the long leg with fewer C domain could form a very stable structure so as not to fall off the track. To verify this hypothesis, we approximately estimated the melting temperature (Tm) of the following three states. Tm of the purely double-stranded hybridization (14 bp) between the C domain of long leg and S was estimated to be 48.1 °C (using the UNAFold 3.9 software and the following input parameters: 5 nM DNA, 50 mM NaCl, and 10 mM $MgCl_2$). When the base number of hybridization increased to 20 bp, the estimated Tm was up to 67.0 °C. In lame walker, one lame catalyst would form a temporarily closed ring with two S chains and the surface of microspheres between S (Fig. S2). In analogy to a hairpin structure, we estimate the Tm with 14 bp of C domain as the stem sequence and a loop containing a number of adenine. The loop bearing a 7 nt T domain, 43 nt spacer, 7 nt short leg and its 7 nt complementary sequence, 16 nt partial sequence of S and the distance between adjacent S accounting for about 6 nt (estimated to be approximately 3 nm based on the information provided by the manufacturer). Thus, the total number of nucleotides in the loop is 86. We finally evaluated the Tm of 14 bp of C domain in the lame walker as 73.8 °C, which is even much higher than that of 14-bp purely double-stranded hybridization. Therefore, it is not surprising that a relatively short C domain could execute the persistence of lame catalyst on the microspheres during walking.

### 3.5. Optimization of the lame DNA walker

In lame walker reaction, the rate-limiting steps rely primarily on the dissociation of the C domain complementary sequence and branch migration with adjacent S through T domain, apart from the cleavage step by Nb.BbvCI. Therefore, we designed six types of catalysts with different lengths of T domain (LT5C14, LT6C14, LT7C14, LT8C14, LT9C14 and LT10C14). In solution, the rate of the branch migration, determined by the binding free energy of the toehold domain, was saturated with the length of toehold about 6–10 nt (Genot et al., 2011; Zhang et al., 2012). We also observed a similar result on the surface of microspheres in Fig. 4A. Although the dissociation of the short T domain (LT5C14) with its complementary sequence was fast, it was not conducive to the toehold exchange mediated branch migration reactions of lame walker due to the low binding free energy of the short T domain. When the length of T domain increased to 7 nt, the lame walker reactions achieved the best performance. Too long toehold (LT10C14), however, inhibited the walker reactions because of slow dissociation of the toehold complementary sequence, resulting in lower fluorescence intensity. Another critical factor for achieving optimum performance of lame walker involved the spacer. As shown in Fig. 4B, a minimum spacer length of 43 nt was required to facilitate coordination between long leg and short leg. The impact of rigid structure of spacer on the performance of the 3-D walker was also measured. We mixed the lame catalyst with its spacer complementary sequence to improve the rigidity of the lame catalyst to a certain extent. We found that the performance of lame walker was independent of rigidity (Fig. S3), which was conducive to the construction of subsequent biosensor.

In addition to the design changes, we also optimized the lame walker by investigating other parameters, including S concentration (Supporting Section 3), enzyme concentration, microsphere concentration and microsphere size. The optimal amounts of S, enzyme, and microsphere were 89 nM, 5 U and 0.5 mg/mL respectively (Fig. 4C and D and 4F). It should be noted that 0.86 μm microspheres could produce a higher endpoint fluorescence signal than 1 μm microspheres in Fig. 4E. The factors leading to the signal variation in fluorescence largely stemmed from differences in curvature effect (Hill et al., 2009). Therefore, 0.86 μm microspheres were used in subsequent experiments (Considering the centrifugal requirements of microsphere size, smaller size microspheres were not selected).

### 3.6. Analytical performance of the lame walker

To apply this technology to the analytical target, GBS T was used as the model target. The bacterial colonies were counted (Fig. S4), together with a set of methods to confirm the existence of GBS based on the

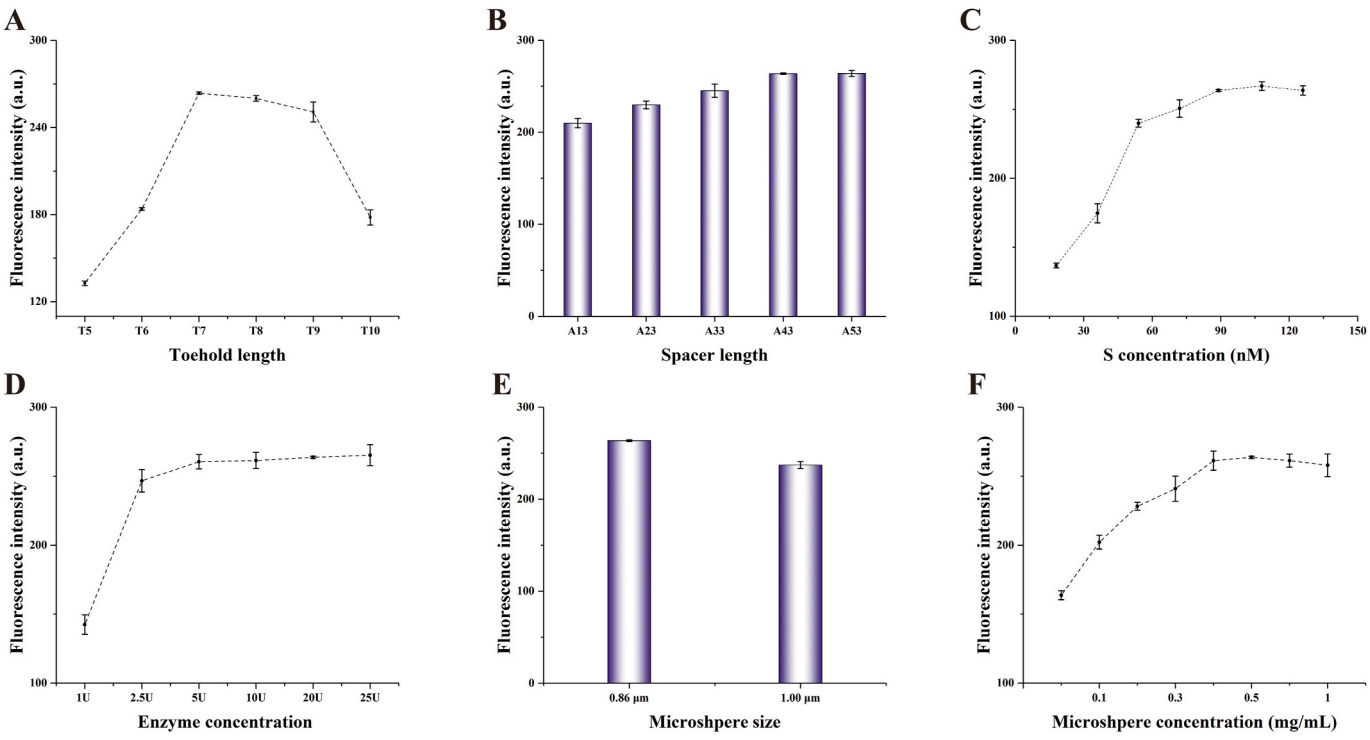


**Fig. 4.** Optimization of the lame walking system. Effect of the length of the T domain (A), spacer length (B), S concentration (C), enzyme concentration (D), microsphere size (E) and microsphere concentration (F) on the performance of the lame walker. Error bars represented one standard deviation from triplicate analyses.

alignment between DNA sequencing and Genbank sequences (Fig. S5). Following addition of GBS T, the lame catalyst from reservoir microspheres was displaced by toehold exchange mechanism. After centrifugation, the free catalyst in the supernatant can then serve as an amplifier to activate subsequent walker reactions (Fig. 5A). We titrated GBS and found the minimum detectable concentration of the lame walker was 10 pM at a signal-to-noise ratio of 3 (Fig. 5B), which was comparable to or even better than most 3-D DNA walkers (Table 1). Linear fitting of target concentration and fluorescence intensity suggested a good correlation in the detection range of 10 pM–5 nM with a correlation coefficient $R^2$ of 0.995 (Fig. 5C). Moreover, the selectivity of the assay was also investigated in the presence of eight potential interfering bacteria. As expected, no significant fluorescent enhancement was observed (Fig. 5D), indicating that our lame walker-based sensor showed high selectivity. We also exploited movement-triggered cascade signal amplification to achieve highly specific and sensitive detection of bacteria DNA (Supporting Section 4). As a proof-of-concept for using this sensor based on the lame walker, our proposed lame DNA walker system showed superior potential for sensing detection.

## 5. Conclusions

Unlike the construction of most double-legged walkers, the lame walker has a long leg mainly responsible for persistent movement and a short leg cutting substrates rapidly. This enzyme-propelled lame walker displays a signal-to-noise ratio of 60.4 in 30 min, showing an advantage over other 3-D DNA walkers. Kinetic studies demonstrate that the average rate of the lame walker can reach $6.467 \times 10^{-11}$ M $s^{-1}$. Besides, Study on the persistence of the lame walker confirms that the lame catalyst does not dissociate—it is only transferred from a split substrate to an adjacent intact substrate on the same microspheres, and is bound to the substrate by hybridization of at least 14 nucleotides. As a proof-of-concept for using this sensor, our proposed lame DNA walker system showed superior potential for sensing detection with high sensitivity and specificity. This work thereby will advance the design of 3-D DNA walkers and substantially contributes to the exploration and application of DNA walking systems.

## Credit author statement

Jie Fang involved in the design, execution of the work and wrote the first draft of the manuscript. Changjing Yuan contributed on concept, interpretation and execution of the work. Junjie Li, Junlong Li, Tingyan Yang, Yongcan Guo, and Ding Wang provided advice and assisted in reviewing the original draft. Prof. Xue, Prof. Fu and Prof. Xie financed and supervised the work.

## Declaration of competing interest

The authors declare that they have no known competing financial

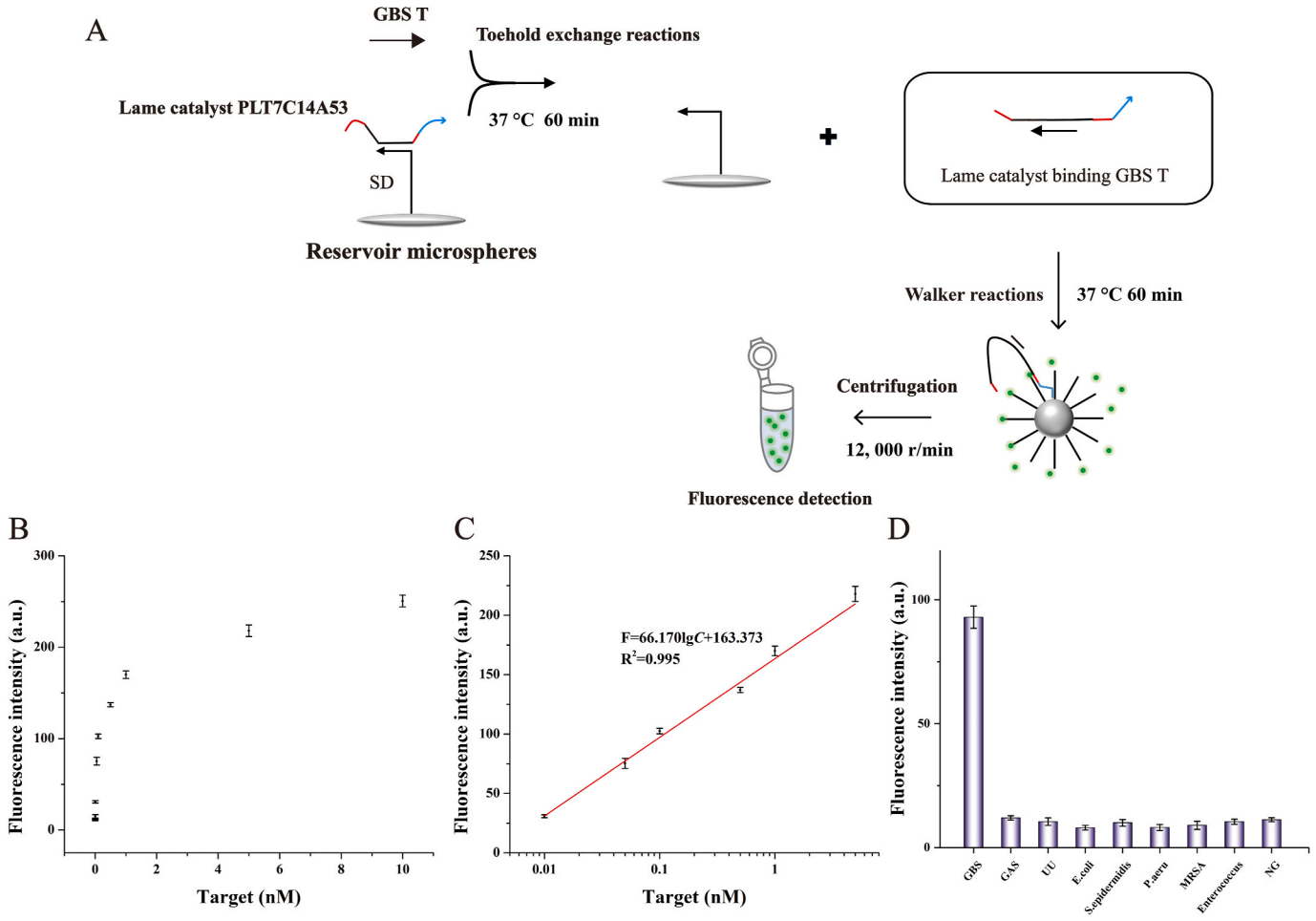


**Fig. 5.** (A) Schematic illustrating the strategy to convert the lame DNA walker into a biosensor for DNA detection. (B) Quantification of GBS T at varying concentrations using end-point fluorescence measured in 60 min and (C) corresponding linear fitting. (D) Selectivity of the assay towards eight interfering bacterial DNA (group A *streptococcus* (GAS), *Ureaplasma urealyticum* (UU), *Escherichia coli* (E.coil), *Staphylococcus epidermidis* (S.epid), *Pseudomonas aeruginosa* (P.aeru), methicillin-resistant *Staphylococcus aureus* (MRSA), *Enterococcus* (ES), and *Neisseria gonorrhoeae* (NG)) at a concentration of 5 nM (The concentration of GBS T was 50 pM). Error bars represented one standard deviation from triplicate analyses.

interests or personal relationships that could have appeared to influence the work reported in this paper.

## Acknowledgements

This work was funded by the National Natural Science Foundation of China (No. 81430054, No. 81672112 and No. 81802112) and Chongqing Technology Innovation and Application Demonstration Project (cstc2018jscx-msybX0010).

## Appendix A. Supplementary data

Supplementary data to this article can be found online at https://doi.org/10.1016/j.bios.2021.112981.

## References

Abendroth, J.M., Bushuyev, O.S., Weiss, P.S., Barrett, C.J., 2015. ACS Nano 9 (8), 7746–7768.
Bath, J., Green, S.J., Allen, K.E., Turberfield, A.J., 2009. Small 5 (13), 1513–1516.
Cha, T.-G., Pan, J., Chen, H., Salgado, J., Li, X., Mao, C., Choi, J.H., 2014. Nat. Nanotechnol. 9 (1), 39–43.
Chai, H., Miao, P., 2019. Anal. Chem. 91 (8), 4953–4957.
Fan, S., Wang, D., Kenaan, A., Cheng, J., Cui, D., Song, J., 2019. Small 15 (26), 1805554.
Feng, C., Wang, Z., Chen, T., Chen, X., Mao, D., Zhao, J., Li, G., 2018. Anal. Chem. 90 (4), 2810–2815.
Genot, A.J., Zhang, D.Y., Bath, J., Turberfield, A.J., 2011. J. Am. Chem. Soc. 133 (7), 2177–2182.
Gu, H., Chao, J., Xiao, S.-J., Seeman, N.C., 2010. Nature 465 (7295), 202–205.
Hill, H.D., Millstone, J.E., Banholzer, M.J., Mirkin, C.A., 2009. ACS Nano 3 (2), 418–424.
Huang, J., Zhu, L., Ju, H., Lei, J., 2019. Anal. Chem. 91 (11), 6981–6985.
Jung, C., Allen, P.B., Ellington, A.D., 2016. Nat. Nanotechnol. 11 (2), 157–163.
Jung, C., Allen, P.B., Ellington, A.D., 2017. ACS Nano 11 (8), 8047–8054.
Li, J., Johnson-Buck, A., Yang, Y.R., Shih, W.M., Yan, H., Walter, N.G., 2018a. Nat. Nanotechnol. 13 (8), 723–729.
Li, N., Zheng, J., Li, C., Wang, X., Ji, X., He, Z., 2017. Chem. Commun. 53 (60), 8486–8488.
Li, S., Chen, N., Zhang, Z., Wang, Y., 2013. Biomaterials 34 (2), 460–469.
Li, Y., Wang, G.A., Mason, S.D., Yang, X., Yu, Z., Tang, Y., Li, F., 2018b. Chem. Sci. 9 (30), 6434–6439.
Liang, C.P., Ma, P.Q., Liu, H., Guo, X., Yin, B.C., Ye, B.C., 2017. Angew. Chem. Int. Ed. 56 (31), 9077–9081.
Liber, M., Tomov, T.E., Tsukanov, R., Berger, Y., Nir, E., 2015. Small 11 (5), 568–575.
Liu, M., Hou, R., Cheng, J., Loh, I.Y., Sreelatha, S., Tey, J.N., Wei, J., Wang, Z., 2014. ACS Nano 8 (2), 1792–1803.
Loh, I.Y., Cheng, J., Tee, S.R., Efremov, A., Wang, Z., 2014. ACS Nano 8 (10), 10293–10304.
Ma, P.Q., Liang, C.P., Zhang, H.H., Yin, B.C., Ye, B.C., 2018. Chem. Sci. 9 (13), 3299–3304.
Muscat, R.A., Bath, J., Turberfield, A.J., 2011. Nano Lett. 11 (3), 982–987.
Pan, J., Cha, T.-G., Li, F., Chen, H., Bragg, N.A., Choi, J.H., 2017. Science advances 3 (1), e1601600.
Shin, J.-S., Pierce, N.A., 2004. J. Am. Chem. Soc. 126 (35), 10834–10835.
Thubagere, A.J., Li, W., Johnson, R.F., Chen, Z., Doroudi, S., Lee, Y.L., Izatt, G., Wittman, S., Srinivas, N., Woods, D., Winfree, E., Qian, L., 2017. Science 357 (6356), eaan6558.
Tian, B., Ma, J., Qiu, Z., Zardan Gomez de la Torre, T., Donolato, M., Hansen, M.F., Svedlindh, P., Stromberg, M., 2017. ACS Nano 11 (2), 1798–1806.
Urban, M.J., Zhou, C., Duan, X., Liu, N., 2015. Nano Lett. 15 (12), 8392–8396.
Wang, D., Vietz, C., Schroder, T., Acuna, G., Lalkens, B., Tinnefeld, P., 2017. Nano Lett. 17 (9), 5368–5374.
Wang, J., 2009. ACS Nano 3 (1), 4–9.
Wang, L., Deng, R., Li, J., 2015. Chem. Sci. 6 (12), 6777–6782.
Wickham, S.F., Endo, M., Katsuda, Y., Hidaka, K., Bath, J., Sugiyama, H., Turberfield, A. J., 2011. Nat. Nanotechnol. 6 (3), 166–169.
Xiao, M., Zou, K., Li, L., Wang, L., Tian, Y., Fan, C., Pei, H., 2019. Angew. Chem. 131 (43), 15594–15600, 2019.
Xu, X., Zhang, P., Zhang, R., Zhang, N., Jiang, W., 2019. Chem. Commun. 55 (43), 6026–6029.
Yang, X., Tang, Y., Mason, S.D., Chen, J., Li, F., 2016. ACS Nano 10 (2), 2324–2330.
Yang, Y., Goetzfried, M.A., Hidaka, K., You, M., Tan, W., Sugiyama, H., Endo, M., 2015. Nano Lett. 15 (10), 6672–6676.
Yehl, K., Mugler, A., Vivek, S., Liu, Y., Zhang, Y., Fan, M., Weeks, E.R., Salaita, K., 2016. Nat. Nanotechnol. 11 (2), 184–190.
Yin, P., Yan, H., Daniell, X.G., Turberfield, A.J., Reif, J.H., 2004. Angew. Chem. 116 (37), 5014–5019.
You, M., Chen, Y., Zhang, X., Liu, H., Wang, R., Wang, K., Williams, K.R., Tan, W., 2012. Angew. Chem. Int. Ed. 51 (10), 2457–2460.
Yuan, C., Fang, J., Duan, Q., Yan, Q., Guo, J., Yuan, T., Yi, G., 2019. Biosens. Bioelectron. 133, 243–249.
Zhang, C., Wang, Z., Liu, Y., Yang, J., Zhang, X., Li, Y., Pan, L., Ke, Y., Yan, H., 2019. J. Am. Chem. Soc. 141 (43), 17189–17197.
Zhang, D.Y., Chen, S.X., Yin, P., 2012. Nat. Chem. 4 (3), 208–214.
Zhang, D.Y., Seelig, G., 2011. Nat. Chem. 3 (2), 103–113.
Zhang, H., Lai, M., Zuehlke, A., Peng, H., Li, X.F., Le, X.C., 2015. Angew. Chem. Int. Ed. 54 (48), 14326–14330.
Zheng, J., Li, N., Li, C., Wang, X., Liu, Y., Mao, G., Ji, X., He, Z., 2018. Biosens. Bioelectron. 107, 40–46.
Zhou, C., Duan, X., Liu, N., 2015. Nat. Commun. 6, 8102.